Modelling Pohang, South Korea, Geothermal Well Stimulations and Seismicity

J.Torquil Smith, Eric L. Sonnenthal, Ernst L. Majer

Lawrence Berkeley National Laboratory

Keywords

Enhanced Geothermal System, induced seismicity, Pohang earthquake, thermal-hydrological-mechanical model

ABSTRACT

The cause of the 5.6 magnitude, 2017 Pohang, S. Korea, earthquake weeks after the end of fluid injection at the co-located Pohang Enhanced Geothermal System project remains controversial. We model the thermal, hydrological and mechanical response to stimulation injections, flow back, and mud-loss volumes in a uniform model with one and two permeable faults suggested by event locations using the Thermal-Hydrological-Mechanical-Chemical code TReactMech. Re-analysis of the events indicates potentially five faults associated with both stimulation events and the 5.6 earthquake aftershocks. One fault intersects the open section of well PX-1 and the mud-loss zone of well PX-2. Neither of the first two modelled faults is connected to the open section of well PX-2. Fault orientations for the five fault model are estimated from planes maximizing the number of events in a thin planar slice. Initial stress ratios of 2.16: 1.12: 1 are based on drilling mud-loss rates and mud densities for the Pohang PX-2 geothermal well, 41 MPa average fluid pressure for expected failure patch area for the Nov 2, 2015, -0.1 magnitude PX-2 mud-loss event, 97.1 MPa vertical stress, stress ratio R=0.9, regional maximum horizontal stress direction N 77 E, fault strike N 146˚ W, 43˚ dip, and measured 0.53 friction coefficient.

Observed cumulative seismic moment associated with mud-loss, and first stimulations in wells PX-2 and PX-1 are roughly matched. Simulation magnitudes for the second stimulation of PX-2 do not approach an observed 3.1 magnitude event. Simulation events for PX-1 stimulation are along the fault intersecting well PX-1 in partial agreement with observed events. Simulation PX-2 stimulation events cluster around open well section, observed events cluster around the modelled faults. Adoption of the five fault model substantially increases the number of events between wells. No large events occur in the simulation after the end of stimulations.

1. Introduction

The relationship of a magnitude 5.6 earthquake coincident with the Pohang geothermal project sixty-one days after the end of stimulation injections there has been much studied (e.g., Lee et al., 2019, Gee et al. 2019). For example, modelling injection in the two wells (PX-1 and PX-2) over the time span of the project, Chang, et al. (2020), find Coulomb stress changes of the order of 250 kPa at an interpreted fault location between the two wells (PX-1, PX-2) at the time of the second treatment (series of stimulation injections) of well PX-1. Yoo et al. (2021) model injection into a fracture in quite impermeable rock on a finer time scale, with dilation and shear of the modelled fracture, and reproduce observed well head pressures for first treatments of the two wells modelled separately quite well.

Here we model injection over the time span of the project, with zones of pre-existing fracture with higher permeability assumed to exist, and assume sufficient fracturing that shear failure and dilation may occur on planes close to the optimal orientation for failure. Integrated seismic energy from shear failure is computed and compared with observed seismicity.

2. Regional Stress

The initial stress state is uncertain. Kim et al. (2017), analyzed well bore break-outs, well damage, and mini-hydraulic fracture data to estimate stresses near 700 m depth in a borehole (exp-1) 3 km from the geothermal project site, and estimated that the vertical stress is the intermediate principal stress there. Lee, et al. (2019) estimate the stresses at 4200 m depth at the geothermal site to be 115-122, 243, 106 MPa, for S_{hmin}, S_{hmax}, S_v, using step rate tests from well PX-2, a Mohr-Coulomb failure condition assumed critical with friction coefficient 0.6, and density measurements from a near-by shallower well, for the three principal stresses respectively, with maximum horizontal stress S_{hmax} estimated to be oriented N 77˚ E, based on borehole dipole sonic data.

We re-estimate maximum horizontal stress based on a large early drilling mud-loss event (M -0.1) at 3800 m depth in PX-2. Given reported mud densities (Lee et al., 2019), mud pressure at 3800 m depth in PX-2 was about 48.6 MPa, and, given an approximately uniform vertical temperature gradient, the hydrostatic pressure there is about 31.7 MPa, so the mud is about 16.9 MPa overpressured. For a -0.1 magnitude event (8.7×10^5 N-m moment), assuming a stress drop of 1 MPa implies about a 6.5 m radius slip patch. About 186 m^3 mud loss occurred Oct 30 to Nov 1, 2015, prior to the -0.1 magnitude micro-earthquake. Under an extremely simplified model of steady slightly compressible fluid flow to cylindrical radius ρ_v = 560 m in a fault treated as a 18 m permeable layer of 0.02 porosity, 1.9×10^{-15} m^2 permeability, with combined pore and fluid compressibility of $4.5\ 10^{-13}$ m^3/Pa (e.g., Hofmann et al., 2019), over pressure varies as $P(\rho) = P_0 \log(\rho_v/\rho) / \log(\rho_v/\rho_0)$, for $\rho_0 \leq \rho \leq \rho_v$, where ρ_0 is the borehole radius (and the total injected fluid is 186 m^3).

Averaging over the 6.5 m radius of the presumed slip area gives an average overpressure of 9.3 MPa, so 41.0 MPa average total pressure. Based on the density model of Lee et al. (2019), vertical stress is 97.1 MPa at 3800 m. Assuming a friction coefficient of 0.53, corresponding to measured core material (Kwon et al. 2019), and stress ratio $R \equiv (\sigma_{max}-\sigma_{inter})/(\sigma_{max}-\sigma_{min}) = 0.9$, corresponding to the value found for Pohang 5.6 magnitude earthquake (Gee et al, 2019), and failure on a plane striking N 214˚ E and dipping 43˚ (to NW), and assuming that the vertical

stress is the minimum stress, yields estimates of S_{hmax} = 209.4 MPa and S_{hmin}= 108.3 MPa, so stress ratios of 2.157: 1.115: 1. This maximum horizontal stress estimate is smaller than that of Lee et al. (2019). One may note that, for a source mechanism for the 5.6 Pohang earthquake with strike N 213.7˚ E, dip 51.2˚, and rake 123.4˚ (Lee et al.) the rake vector, which is direction of motion of the upper fault surface, is (0.244, 0.753, 0.611) (N, E, up), this resolves into components -0.621 in the strike direction and -0.784 in the dip direction, so the motion is more over thrust than strike slip, supporting identification of vertical as the minimum stress direction. The preponderance of over thrust to strike slip motion is supported by fault slip modelling of 3-D interferometric synthetic aperture radar (InSAR) data reported in Lee et al.

3. Faulting

Three models of faulting in the study area are used. The first is a single fault striking N 214˚ E, dipping 43˚, intersecting the PX-2 drill hole at 3800 m depth, where major mud loss occurred in PX-2 before it was cased, with extent 1500 x 900 m, following Chang, et al. (2020). The second is the same as the first, but with an overlying second fault, suggested by cross sections of stimulation-induced seismicity (Lee et al., 2019) dipping 32˚, 960 x 960 m, and intersecting the uncased section of well PX-1 at about 4100 m depth.

For the third faulting model, 95 stimulation and mud loss micro-earthquake locations (from Lee et al.) were analyzed for alignment on planes. A grid was systematically searched for the maximum number of located events within any 30 m slice, as a function of slice normal orientation. The maximum number of events in a slice is plotted in Figure (1). There is a clear maximum at fault plane normal orientation N 117˚ E with fault dip 21˚, with 32 located events in the slice. The grouping has approximate length 1.0 km and breadth 0.8 km based on the variance of locations in strike and dip directions. Events in this slice were removed and the process repeated to estimate two additional sets of coplanar events. Fault details are given in Table (1). None of these corresponds to the planes initially modelled, nor to the fault plane of the 5.6 magnitude event inferred from it source mechanism.

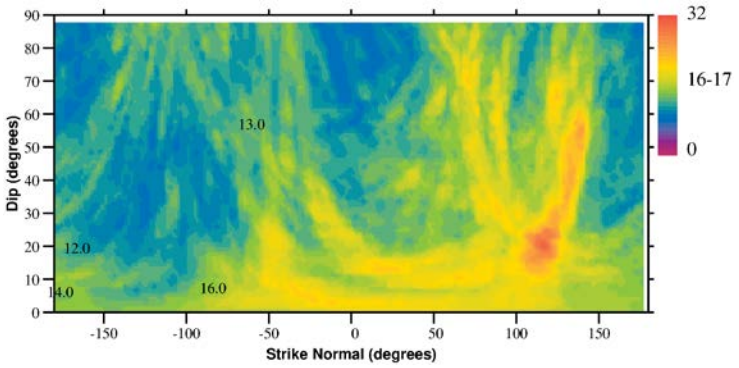

Figure 1: Maximum number of stimulation micro-earthquakes in 30 m thick zone, as function of plane normal azimuth and plane dip.

Table 1. Maximum stimulation MEQ density planes, in order of abstraction from pool of 95 events. Center locations in coordinates centered at 36.109˚ N, 129.374˚ E. Length and breadth approximate, based on variance of member event coordinates.

#	Strike (˚)	Dip (˚)	North (m)	East (m)	Up (m)	# events	length (km)	breadth (km)
1	N 207˚ E	21˚	-112	-30	-4138	32	1.0	0.8
2	N 160˚ E	70˚	153	-29	-4120	18	1.0	0.7
3	N 166˚ E	36˚	24	35	-4091	12	0.9	0.7

Consequently, the process was repeated on a set of 280 locations of aftershocks to the 5.6 magnitude event, determined by researchers at the Korea Institute of Geoscience and Mineral Resources. The orientation of planes with maximum number of events in any 100 m thick zone was determined, and repeated 5 times in succession, with removal of contained events at each stage, to give a set of 6 planes of concentrated events, presumably fault planes, given in Table 2. Four of these are similar to 4 planes fit to 1132 aftershocks relocated and analyzed by Son et al. (2020); planes 6, 1, 5, and 2, differ in orientation by 6˚, 16˚, 8˚ and 13˚ from estimates of Son, et al. Plane 4 is the closest in orientation to the fault plane of the 5.6 magnitude main shock estimated from source mechanism, differing by 16˚ from the Lee, et al., estimate, and by 7˚ from that of Son, et al. Planes 4 and 6 lie in the modelled domain.

Table 2. Maximum aftershock density planes, in order of abstraction from pool of 280 events. Center locations in coordinates centered at 36.109˚ N, 129.374˚ E.

#	Strike (˚)	Dip (˚)	North (m)	East (m)	Up (m)	# events	length (km)	breadth (km)
1	N 216 E	77	-885	-1538	-3776	39	7.9	4.4
2	N 31 E	66	-673	-1941	-4298	36	11.9	2.6
3	N 204 E	78	128	-1020	-3823	29	8.0	3.7
4	N 228.5 E	58	-422	-910	-3226	26	8.3	3.4
5	N 223 E	82.5	-826	-1799	-3339	21	5.8	3.7
6	N 229 E	63	-1084	-1341	-4195	18	5.5	3.2

4. Simulation

We restricted our modelling to a 4 x 4 x 4 km volume immediately surrounding the Pohang geothermal development site. Elastic moduli, density, and Mohr Coulomb dilation for core material from the 4200 m depth level (Kwon et al., 2019), were used for the background rock. Background and fault rock permeability was from Chang et al. (2019). Fault permeability was checked for consistency with average mud loss rate at 4065 m depth in well PX-1 and mud pressure determined by mud densities (from Lee et al. 2019), assuming a 34 m thick permeable fault zone. The initial model consists of one fault zone dipping 43˚, with strike N 214˚ E consistent with the source mechanism for the 5.6 November 15, 2017 Pohang earthquake, following Chang, et al. The modelling grid was aligned with the presumed strike direction. Open well section locations relative to the modelled fault zones were determined from description in Chang et al., Ge et al. (2019), and Hoffman et al. (2019). Initial temperature was determined by linear interpolation to model boundaries, of an average nearby shallow well temperatures, and a pre-exploitation 180 ˚C temperature at 5 km depth (Lee et al.), and subsequent simulation

approaching long term equilibrium. Measured injection volumes and flow backs were averaged to hourly average values, and mud loss rates were estimated from daily mud loss plots (in Lee et al.), and injected and/or produced from a gridded version of the modelled domain, using Thermal-Hydrological-Mechanical-Chemical modelling program TReactMech (Kim et al., 2012, Smith et al., 2015). Injected water reaching the open section was assumed to be 154 ˚C, mid-way between surface and 4200 m depth temperatures. Injection-flow back volumes are plotted in Figure (2).

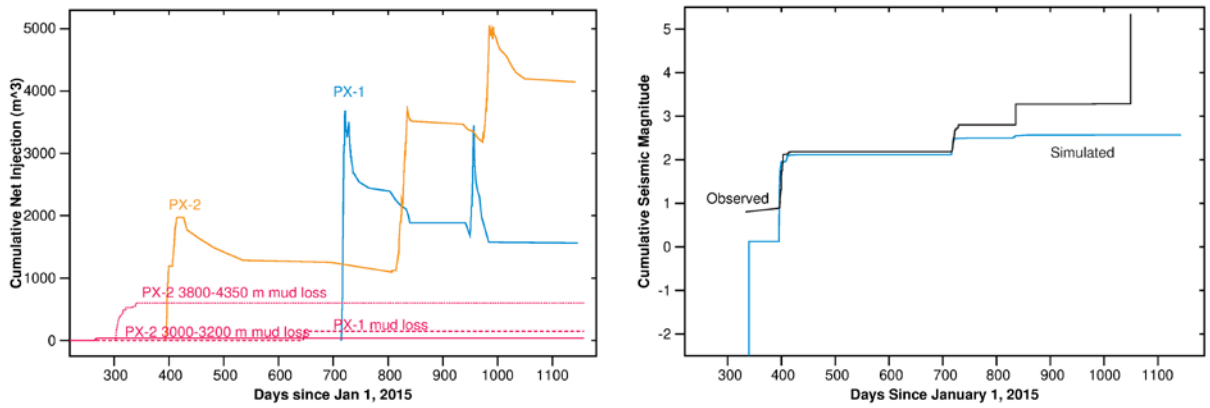

Figure 2. (Left) Cumulative injection less flow back, and mud losses. (Right) Cumulative seismic moment, observed, and simulated for one dipping permeable fault.

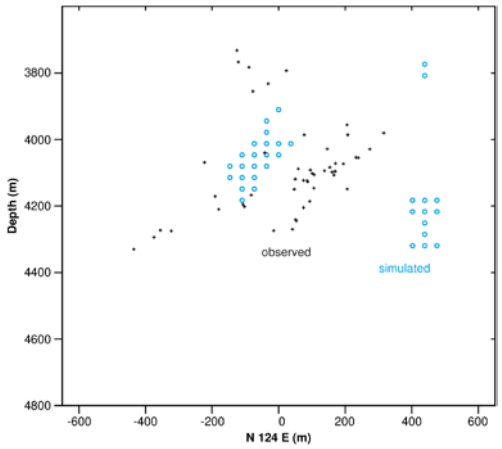

Figure 3. (Projection of) stimulation micro-earthquake locations on vertical plane (blue), for two fault plane model, and observed MEQs (during stimulations) with magnitude 0.5 or greater (black). (Modelling grid discretization evident.)

Simulation of the single fault model results in micro-earthquakes (MEQs) due to mud loss in well PX-2 between 3800 and 4350 m depth, in year 2015, (Julian) days 303-339, the first injections in PX-2, days 394-416, first in PX-1, days 715-728, second PX-2, days 806-835 (very slight), second PX-1, days 950-957 (none), and third PX-2, days 973-992 (very slight). Simulation of the seismic moment was calculated from the product of the simulation failure shear, strain element volume and shear modulus, as integration of (failure) shear strain across an element gives the shear and this is then weighted by the area normal to that. Observed and computed cumulative seismic magnitude (sum of earthquake energies expressed as magnitude of single earthquake of equal energy, on a logarithmic scale) are plotted in Figure 2. Plots of MEQ

locations (not shown) cluster around open well (injection) segments, and mud-loss locations, but fail to capture observed MEQ activity between wells. The second interpreted fault dipping 42˚ mentioned in the previous section, was added, intersecting the PX-1 open well section. Simulation MEQs and observed MEQs with magnitude 0.5 or larger are shown in Figure 3 in projection on a vertical plane. Simulation events occur in three groups, one around the intersection of the added fault with open PX-1 well bore (with a slanting configuration), one about the open section of well PX-2 (about 400 m N 124˚ E), and one at the location the mud loss at 3800 m depth in well PX-2. Simulation events are plotted at element centers, and the discretization of the modelling grid is evident. Most observed events are considerably separated from the open well bore sections, whereas simulation events are not.

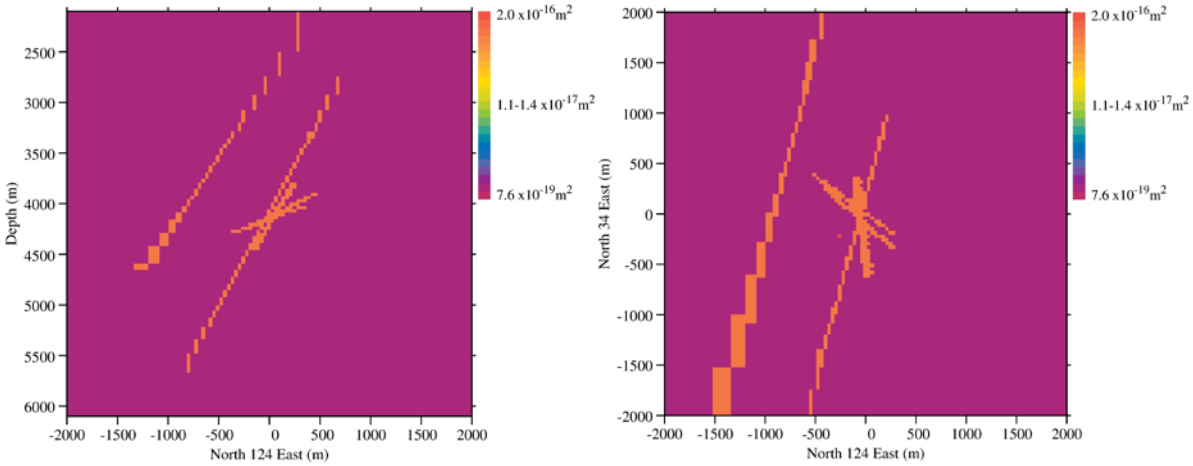

Figure 4. Vertical permeability model vertical cross section (left) centered on latitude 36.109˚ N, longitude 129.374˚ E, and horizontal cross section (right) through 4167 m depth, intersecting aftershock planes 4 and 5 (longer 'lines'), and stimulation MEQ planes 1-3 (shorter 'lines'). Element with well PX-1 open section visible in horizontal section at -252 m N 124˚ E, -216 m N 34˚ E. Open section for well PX-2 begins roughly 30 m below the horizontal plane shown, at approximately 335 m N 124˚ E and -80 m N 34˚ E.

In the hope of better simulating the observed distribution of MEQs, analyses of stimulation MEQ and 5.6 Pohang earthquake aftershock locations in the previous section were made to obtain a more accurate location of (presumably) permeable fault locations. A model was constructed with permeable faults in the 3 planes found from the stimulation MEQs (Table 1), and planes 4 and 6 from the aftershock sequences (Table 2). Faults were modelled as rectangular with the estimated dimensions. Vertical permeability is shown in vertical cross section and horizontal section at 4167 m depth in Figure 4. Cumulative seismic magnitude for simulation in this model is plotted in Figure 5. Response to the well PX-2 mud loss between 3800 and 4350 m depth, in Julian days 303-339, is substantially greater, so the cumulative curve is somewhat lifted, particularly after the first well PX-2 stimulation, days 394-416. After the first stimulation in PX-1, days 715-728, the contribution of the early mud-loss event is smaller relative to the cumulative curve, and the curve is less shifted on the (logarithmic) magnitude scale. Location of simulation MEQs is shown in Figure 6. Simulation MEQs again are solely in the vicinity of the open sections of well, and mud loss zone, as in Figure 3.

In these simulations, failure has been assumed to occur on pre-existing fractures oriented on the failure planes of maximum Coulomb failure criterion (Coulomb stress) assuming zero cohesion.

All failure in the current simulations is shear failure, and shearing is assumed to occur with the 3.4˚ dilation angle measured for core material from 4200 m depth (Kwon, et al., 2019). This produces an increase in porosity, and presumed increase in permeability. Conversion of the increase in porosity to increase in permeability involves assuming a fracture spacing, or alternatively, a proportion of porosity considered to be due to connected fractures. In the current examples 0.1 of the material porosity (0.0048 for the background rock) is assumed to be in connected fractures, implying a fracture porosity of 0.00048. For 7.6×10^{-19} m^2 permeability rock this implies an extremely close fracture spacing. Core extracted from 4200 m depth in PX-2, had an average of 9.7 fractures/m (Kwon, et al.), or a fracture spacing of about 0.1 m. However, one

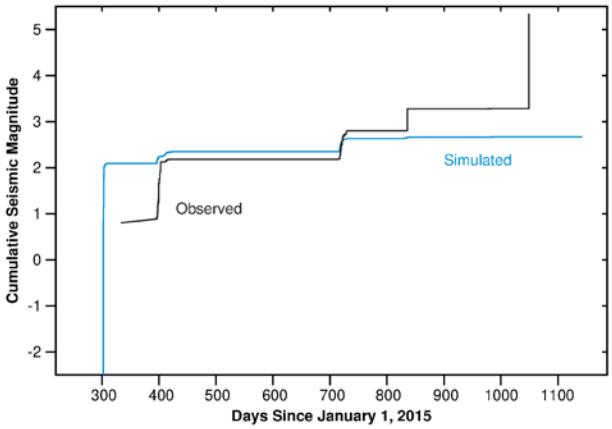

Figure 5. Cumulative seismic moment, observed and simulated for five fault model with three stimulation MEQ fault planes and two aftershock fault planes, assuming very fine fracture spacing.

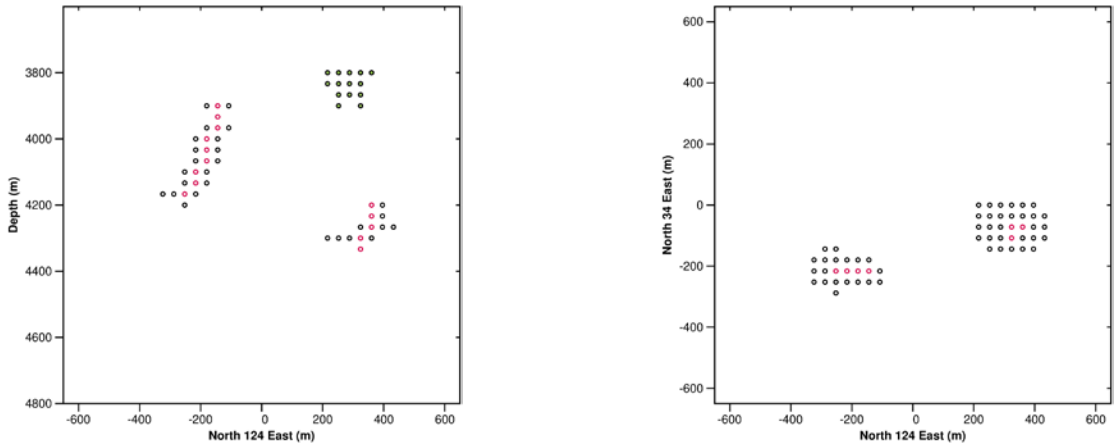

Figure 6. Five fault simulation MEQ locations, (left) projection on vertical plane, (right) projection on horizontal plane. Cells with open well are red (PX-1 left cluster, PX-2 right cluster)

expects core to shatter the during drilling and coring, due to variations in stress components much greater than material cohesion. Thus, a larger spacing seems appropriate. Lee, et al. (2019) report fault gouge in 84 out of 500 one meter segments reported. Assuming one fracture per interval with gouge, implies an average fracture spacing of 6 m, is perhaps a more realistic estimate of fracture spacing. The five fault model has been run with this fracture spacing assumed for computation of permeability changes from fracture dilation on shearing. This results in substantially greater permeability enhancement, and failure further from the open well sections, but still with failing elements (MEQ locations) directly around the open sections.

Cumulative seismic magnitude is plotted for this in Figure 7. The large increase in seismicity due to the first PX-2 stimulation (days 394-416) is primarily due to a reduction in the maximum time step allowed from 3 hours to 1 hour. In the modelling, permeability changes with failure are applied to the flow modelling on the succeeding time step, and thus are applied sooner with the smaller maximum time steps. The evident difference indicates that the previous results above must be interpreted as tentative, as the time stepping was too coarse. Simulation micro-seismic activity is plotted in Figure 8, with color according to presence of faults from Table 1 or 2. (Cells from faults with fewer failing cells plotted preferentially.) This is considerably more spread out than in the simulation plotted in Figure 6. This is primarily due to the increase in the fracture spacing assumed in permeability increase on failure, rather than to the change in maximum time step size- an identical run without the reduction in maximum time step size (not shown) has similar micro-seismic activity distribution plots, although differing in detail. With the assumption of 6 m fracture spacing, micro-seismic activity begins to propagate into the fault zones indicated by stimulation MEQs (Table 1) and by the aftershock sequences (Table 2), although still not reproducing the geometry of the observed micro-earthquakes which are also plotted in Figure 8 for comparison.

In all case, modelling fails to find the large increase in seismicity with the second well PX-2 stimulation, much less the 5.6 magnitude event after the end of stimulation, suggesting perhaps, spatial variation in pre-existing stress.

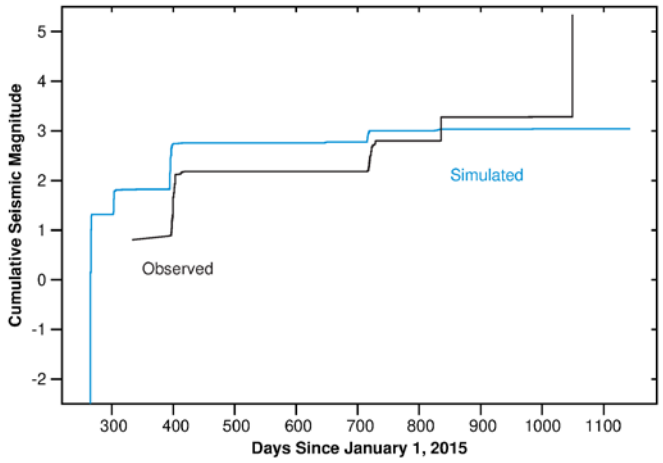

Figure 7. Cumulative seismic moment for 5 faults model, with permeability changes on failure assuming 6 m fracture spacing.

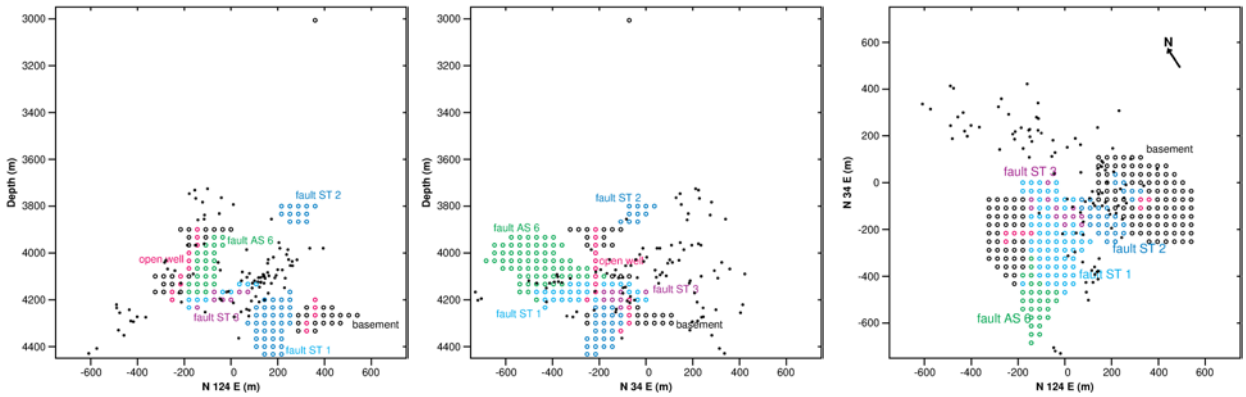

Figure 8. Five fault simulation MEQ locations, with permeability changes assuming 6 m fracture spacing. (Left) projection on vertical plane striking N 124 E, (middle) projection on vertical plane striking N 34 E, (right) projection on horizontal plane. Red; cells with open well (PX-1 left, PX-2 right in each view). Black; cells with background basement rock. Green; cells with Table 2, fault 6. Light blue; cells with Table 1, fault 1. Darker blue; cells with Table 1, fault 2. Purple; cells with Table 1, fault 3. Small black circles; observed MEQs.

Conclusions

Simulations assuming a very high fracture density in computing the effect of shear movement (failure) on permeability estimate a low change in permeability, and pressure perturbations do not penetrate sufficiently away from the wells to replicate the observed co-stimulation micro-seismicity. Assuming a moderate fracture density (6 m fracture spacing) based on the relative frequency of gouge in 1 m intervals reported between 3116 and 4218 m depth, results in substantially higher changes in permeability allowing pressure changes to penetrate further from the wells, and induce shearing there. With adoption of a five fault model, the distribution of simulated seismicity begins to approach the seismicity observed during stimulation, though fails to predict the magnitude of seismicity induced by the second stimulation of well PX-2, and altogether fails to predict the 5.6 magnitude earthquake 61 days after the end of stimulation injections. This is perhaps, in part, a consequence of the rather conservative regional stress estimate used, based on analysis of an early drilling mud-loss event in PX-2. This together with a fairly different stress ratio estimated at much shallower depths suggest that the assumption of constant initial stress ratios over the modelled volume may be a fairly rough approximation.

Acknowledgement

This work was supported by D.O.E. contract.

REFERENCES

Chang, K.W., Yoon, H., Kim, Y., and Lee, M.Y., 2020, "Operational and geological controls of coupled poroelastic stressing and pore-pressure accumulation along faults: induced earthquakes in Pohang, South Korea", Nature Research, Scientific Reports, 10:2073,

Gee, S., Ellsworth, W. L., Giardini, D., Townsend, J., and, Shimamoto, T., 2019, "Overseas Research Advisory Committee Report on the Pohang Earthquake". The Geological Society of Korea, Korean Government Commission on the Cause of the Pohang Earthquake.

Hofmann, H., Zimmermann, G., Farkas, M., Huenges, E, Zang, A., Leonhardt, M., Kwiatek, G., Martinez-Garzon, P., Bohnhoff, M., Min, K., Fokker, P., Westaway, R., Bethmann, F., Meier, P., Yoon, K.S., Choi, J.W. , Lee, T.J. and Kim, K.Y., 2019, "First field application of cyclic soft stimulation at the Pohang enhanced geothermal system site in Korea", Geophys. J. Int.(2019), vol. 217, 926-949.

Kim, H., Xie, L., Min, K., Bae, S., and Stephansson, O., 2017, "Integrated in situ stress estimation by hydraulic fracturing, borehole observations and numerical analysis at the Exp-1 borehole in Pohang, Korea", Rock Mech Rock Eng (2017) 50, 3141-3155.

Kim, J., Sonnenthal, E.L., and Rutqvist, J., 2012, "Formulation and sequential numerical algorithms of coupled fluid/heat flow and geomechanics for multiple porosity materials", Int. J. Numer. Meth. Engng., 92, pp 425-456.

Kwon, S., Xie, L., Park, S., Kim, K., Min, K., Kim, K.Y., Zhuang, L., Choi, J., Kim, K., and Lee, T.J., 2019, "Characterization of 4.2-km deep fractured granodiorite cores from Pohang geothermal reservoir, Korea". Rock Mechanical and Rock Engineering 52 (1), 771-782.

Lee, K., Yeo, I., Lee, J., Kang, T., Rhie, J., Sheen, D., Chan, C., Son, M., Cho, I., Oh, S., Pyun, S., and Kim, S., 2019, "Final Report of the Korean Government Commission on Relations Between the 2017 Pohang Earthquake and EGS Project". The Geological Society of Korea, Korean Government Commission on the Cause of the Pohang Earthquake. (In Korean, with chapter abstracts, table captions, figure captions and assorted phrases in English. Earlier version summarized in part in Gee et al., 2019).

Smith, J.T., Sonnenthal, E.L., and Trenton, C., 2015, "Thermal-hydrological-mechanical modelling of shear stimulation at Newberry Volcano, Oregon". Proceedings of 49th US Rock Mechanics/Geomechanics Symposium of the American Rock Mechanics Association, San Francisco, Calif., ARMA 15-0680.

Son, M., Cho, C.S., Lee, H.K., Han, M., Shin, J.S., Kim, K., and Kim, S., 2020, "Partitioned fault movement and aftershock triggering: evidence for fault interactions during the 2017 Mw5.4 Pohang earthquake, South Korea". JGR Solid Earth, 10.1029/2020JB020005